AD735963

MONTE CARLO TRAJECTORY CALCULATIONS
OF THE DISSOCIATION OF HCl IN Ar

by

Ven H. Shui, John P. Appleton and James C. Keck

November 1971

FLUID MECHANICS LABORATORY

JAN 28 1972

DDC

DEPARTMENT OF MECHANICAL ENGINEERING

MASSACHUSETTS INSTITUTE OF TECHNOLOGY

DOCUMENT CONTROL DATA - R&D

(Security classification of title, body of abstract and indexing annotation must be entered when the overall report is classified)

1. ORIGINATING ACTIVITY (Corporate author)	2a. REPORT SECURITY CLASSIFICATION
Massachusetts Institute of Technology Cambridge, Massachusetts	Unclassified
	2b. GROUP Fluid Mechanics Laboratory

3. REPORT TITLE

Monte Carlo Trajectory Calculations of the Dissociation of HCl in Ar

4. DESCRIPTIVE NOTES (Type of report and inclusive dates)

5. AUTHOR(S) (Last name, first name, initial)

Ven H. Shui, John P. Appleton and James C. Keck

6. REPORT DATE	7a. TOTAL NO. OF PAGES	7b. NO. OF REFS
November 1971	35	23

8a. CONTRACT OR GRANT NO.	9a. ORIGINATOR'S REPORT NUMBER(S)
N0014-67-A-0204-0040	Fluid Mechanics Laboratory
b. PROJECT NO. ARPA Order No. 322	Publication No. 71-15
c.	9b. OTHER REPORT NO(S) (Any other numbers that may be assigned this report)
d.	

10. AVAILABILITY/LIMITATION NOTICES

Distribution Unlimited

11. SUPPLEMENTARY NOTES	12. SPONSORING MILITARY ACTIVITY
	Advanced Research Projects Agency of the Department of Defense and monitored by the Office of Naval Research

13. ABSTRACT

The modified phase-space theory of reaction rates is applied to the dissociation of HCl in a heat bath of argon atoms. Excellent agreement is obtained between the theoretical predictions and the shock-tube measurements of the dissociation rate coefficient over the temperature range 2500-5000 $^\circ$K. The recrossing correction factor and nonequilibrium correction factor are obtained from Monte Carlo trajectory calculations for states near the dissociation limit. The trajectories were sampled within the reaction zone, with a weight proportional to the equilibrium reaction rate, and numerically integrated in both time-wise directions to determine the complete histories of the collisions. A simple separable function for the equilibrium transition rate $R(\epsilon_i, \epsilon_f)$ from initial states ϵ_i to final states ϵ_f was obtained to fit the numerical data with sufficient accuracy and was used to solve the steady-state master equation. Important features of collisions of highly asymmetric diatomic molecules are discussed, and several typical reactive trajectories are shown to illustrate the importance of rotational motion in such collisions.

DD FORM **1473**
1 JAN 64

14. KEY WORDS	LINK A		LINK B		LINK C	
	ROLE	WT	ROLE	WT	ROLE	WT
1. Chemical Kinetics						
2. Dissociation						
3. Hydrogen Chloride						
4. Monte Carlo Calculation						
5. Phase-space Theory						
6. Reaction Rates						
7. Recombination						

INSTRUCTIONS

1. ORIGINATING ACTIVITY: Enter the name and address of the contractor, subcontractor, grantee, Department of Defense activity or other organization (corporate author) issuing the report.

2a. REPORT SECURITY CLASSIFICATION: Enter the overall security classification of the report. Indicate whether "Restricted Data" is included. Marking is to be in accordance with appropriate security regulations.

2b. GROUP: Automatic downgrading is specified in DoD Directive 5200.10 and Armed Forces Industrial Manual. Enter the group number. Also, when applicable, show that optional markings have been used for Group 3 and Group 4 as authorized.

3. REPORT TITLE: Enter the complete report title in all capital letters. Titles in all cases should be unclassified. If a meaningful title cannot be selected without classification, show title classification in all capitals in parenthesis immediately following the title.

4. DESCRIPTIVE NOTES: If appropriate, enter the type of report, e.g., interim, progress, summary, annual, or final. Give the inclusive dates when a specific reporting period is covered.

5. AUTHOR(S): Enter the name(s) of author(s) as shown on or in the report. Enter last name, first name, middle initial. If military, show rank and branch of service. The name of the principal author is an absolute minimum requirement.

6. REPORT DATE: Enter the date of the report as day, month, year; or month, year. If more than one date appears on the report, use date of publication.

7a. TOTAL NUMBER OF PAGES: The total page count should follow normal pagination procedures, i.e., enter the number of pages containing information.

7b. NUMBER OF REFERENCES: Enter the total number of references cited in the report.

8a. CONTRACT OR GRANT NUMBER: If appropriate, enter the applicable number of the contract or grant under which the report was written.

8b, 8c, & 8d. PROJECT NUMBER: Enter the appropriate military department identification, such as project number, subproject number, system numbers, task number, etc.

9a. ORIGINATOR'S REPORT NUMBER(S): Enter the official report number by which the document will be identified and controlled by the originating activity. This number must be unique to this report.

9b. OTHER REPORT NUMBER(S): If the report has been assigned any other report numbers (either by the originator or by the sponsor), also enter this number(s).

10. AVAILABILITY/LIMITATION NOTICES: Enter any limitations on further dissemination of the report, other than those imposed by security classification, using standard statements such as:

  (1) "Qualified requesters may obtain copies of this report from DDC."

  (2) "Foreign announcement and dissemination of this report by DDC is not authorized."

  (3) "U. S. Government agencies may obtain copies of this report directly from DDC. Other qualified DDC users shall request through
  _____ ."

  (4) "U. S. military agencies may obtain copies of this report directly from DDC. Other qualified users shall request through
  _____ ."

  (5) "All distribution of this report is controlled. Qualified DDC users shall request through
  _____ ."

If the report has been furnished to the Office of Technical Services, Department of Commerce, for sale to the public, indicate this fact and enter the price, if known.

11. SUPPLEMENTARY NOTES: Use for additional explanatory notes.

12. SPONSORING MILITARY ACTIVITY: Enter the name of the departmental project office or laboratory sponsoring (paying for) the research and development. Include address.

13. ABSTRACT: Enter an abstract giving a brief and factual summary of the document indicative of the report, even though it may also appear elsewhere in the body of the technical report. If additional space is required, a continuation sheet shall be attached.

It is highly desirable that the abstract of classified reports be unclassified. Each paragraph of the abstract shall end with an indication of the military security classification of the information in the paragraph, represented as (TS), (S), (C), or (U).

There is no limitation on the length of the abstract. However, the suggested length is from 150 to 225 words.

14. KEY WORDS: Key words are technically meaningful terms or short phrases that characterize a report and may be used as index entries for cataloging the report. Key words must be selected so that no security classification is required. Identifiers, such as equipment model designation, trade name, military project code name, geographic location, may be used as key words but will be followed by an indication of technical context. The assignment of links, rules, and weights is optional.

MONTE CARLO TRAJECTORY CALCULATIONS OF THE DISSOCIATION OF HCl IN Ar

by

Ven H. Shui, John P. Appleton and James C. Keck

Fluid Mechanics Laboratory

Department of Mechanical Engineering
Massachusetts Institute of Technology

November 1971

Monte Carlo Trajectory Calculations of the Dissociation of HCl in Ar[*]

by

Ven H. Shui, John P. Appleton and James C. Keck
Massachusetts Institute of Technology, Cambridge, Massachusetts

ABSTRACT

The modified phase-space theory of reaction rates is applied to the dissociation of HCl in a heat bath of argon atoms. Excellent agreement is obtained between the theoretical predictions and the shock-tube measurements of the dissociation rate coefficient over the temperature range 2500-5000 $^{\circ}$K. The recrossing correction factor and nonequilibrium correction factor are obtained from Monte Carlo trajectory calculations for states near the dissociation limit. The trajectories were sampled within the reaction zone, with a weight proportional to the equilibrium reaction rate, and numerically integrated in both time-wise directions to determine the complete histories of the collisions. A simple separable function for the equilibrium transition rate $R(\varepsilon_i, \varepsilon_f)$ from initial states ε_i to final states ε_f was obtained to fit the numerical data with sufficient accuracy

and was used to solve the steady-state master equation. Important features of collisions of highly asymmetric diatomic molecules are discussed, and several typical reactive trajectories are shown to illustrate the importance of rotational motion in such collisions.

I. INTRODUCTION

The modified phase-space theory of reaction rates has been developed by Keck and his co-workers[1-5] and applied quite successfully to the three-body recombination and dissociation of diatomic molecules which have similar atomic masses. However, as demonstrated by Shui, Appleton, and Keck,[4] the theoretical predictions of the dissociation rate coefficients k_d for HF and HCl are much too low by comparison with experimental measurements (see Figures 9 and 10 of Reference 4), although the barrier rate coefficients k_d^B lie above the experimental measurements and have about the right temperature dependence. The reason for this disagreement was believed to be that the estimates of the recrossing correction factors $(N/N_o) \lesssim 0.01$, and the nonequilibrium correction factors $(k/k_e) \simeq 0.01$ were too small.

The correlation formulae used in Reference 4 to estimate the values of (N/N_o) and (k/k_e) were deduced using the results of Monte Carlo trajectory calculations[6] and master equation solutions[7] in which the recombining (dissociating) molecules had atoms of similar masses. It was suggested[4] that the mechanics of reacting collision processes in which one of the recombining atoms had a very small mass, such as the hydrogen halides, was sufficiently different from those cases considered in References 6 and 7, that the correlation formulae were no longer valid.

This paper presents results of Monte Carlo trajectory calculations for the HCℓ + Ar system, and from these, determinations were made of the dissociation rate coefficients which could be compared with shock-tube measurements. In Section II the equations and statistical methods used to obtain the numerical results are derived and summarized. Section III presents a summary of the results and their comparison with the experimental measurements, and Section IV contains our concluding discussion.

II. MONTE CARLO TRAJECTORY CALCULATIONS

The steady state reaction rate coefficient k (subscript r for recombination; d for dissociation) is given by the relationship

$$k = k^B \ (N/N_o) \ (k/k_e) \tag{2.1}$$

where the "barrier" rate coefficient k^B is defined as

$$k^B = \mathscr{R}_v(0)/V \ \Pi[M_j] \ . \tag{2.2}$$

In Equation (2.2), V is the normalization volume in configuration space, $[M_j]$ is the concentration of particles of type M_j in the initial state,

$$\mathscr{R}_v(\epsilon) = \int_{S(\epsilon)} \rho(\vec{v} \cdot \vec{n}) \ ds \tag{2.3}$$

is the "variational rate" (see Reference 2) for the surface S(c) defined by

$$(H - B)/kT = c \ , \tag{2.4}$$

and the corresponding equilibrium one-way crossing rate $\mathscr{R}(\epsilon)$ is given by the expression

$$\mathscr{R}(\epsilon) = (N/N_o) \cdot \mathscr{R}_v(\epsilon)$$

Here, ρ is the density of the representative points, $\vec{v}$ is the generalized velocity, $\vec{n}$ is the unit outward normal to ds, and B and H are the barrier

height and Hamiltonian of the molecule, respectively. As implied by Equation (2.4), the energy (ϵ) of the molecule is measured from the top of the rotational barrier. Other definitions and more detailed descriptions can be found in References 2 and 3.

Monte Carlo trajectory calculations as applied here efficiently evaluate the correction factors (N/N_o) and (k/k_e) by statistically sampling within the reaction zone and numerically integrating the classical equations of motion in both time-wise directions to determine the complete history of the collisions. By sampling with a weight proportional to the local flow rate $\rho(\vec{v} \cdot \vec{n})$ across the surface $S(\epsilon)$, a statistical distribution of trajectories is obtained which reflects their a priori contribution to the reaction rate, thus enabling calculations to be made of the correction factors without further weighting. The representative points were selected from the reaction zone region, i.e., on the surface $S(\epsilon)$, and the equations of motion were integrated outwards in both time-wise directions and terminated as soon as the interaction with the third body became negligible. This avoided unnecessary integrations in regions where interactions were very weak and inconsequential to the outcome of the collisions.

IIA. Recrossing Correction Factor

The N_o trajectories sampled which cross the barrier surface, $\epsilon = 0$, can be divided into four categories, i.e., f → b, f → f, b → b, and b → f, depending on whether the initial and final states of the molecule are free (f) or bound (b). The f → b trajectories are "reactive" (in terms of recombination) while the others are all regarded as being "non-reactive." The recrossing correction factor (N/N_o) is

then given by the expression[6]

$$N/N_o = \sum_n [N(f|n|b)/n]/N_o \qquad (2.6)$$

where N is the effective number of reactive trajectories and $N(f|n|b)$ is the number of trajectories that go from a free state f to a bound state b with n crossings of the barrier surface in the direction $f \to b$, and $n - 1$ crossings in the direction $b \to f$.

IIB. Transition Rates and Nonequilibrium Correction Factors

The nonequilibrium correction factor (k/k_e) is the ratio between the steady state reaction rate and the corresponding equilibrium reaction rate coefficient. Keck and Carrier[7] investigated the coupled vibration-dissociation-recombination process for gas mixtures which consisted primarily of diatomic molecules highly diluted in a heat bath of inert gas atoms such as argon. They presented techniques for solving the appropriate master equations and showed that great simplifications could be obtained if the kernel $R(\varepsilon_i, \varepsilon_f)$ in the master equation was separable. The kernel $R(\varepsilon_i, \varepsilon_f)$ is the "one-way" equilibrium transition rate between energy states $\varepsilon = \varepsilon_i$, and $\varepsilon = \varepsilon_f$, per unit volume, per unit initial and final energies. The energies are measured in the units of kT.

Monte Carlo trajectory calculations were first used to generate a relative numerical distribution of $R(\varepsilon_i, \varepsilon_f)$ as a function of ε_i and ε_f. A functional form for $R(\varepsilon_i, \varepsilon_f)$ was then obtained by a suitable fitting procedure which approximated the numerical distribution. This functional form was used, following Keck and Carrier's analysis,[7] to solve the appropriate master equation and thus to obtain the corresponding nonequilibrium correction factors k/k_e.

The method of generating the relative numerical distributions of $R(\varepsilon_i, \varepsilon_f)$ from Monte Carlo trajectory calculations employed was similar to that used by Mansbach and Keck[8] which they applied to the problem of atomic excitation and ionization by thermal electrons. Briefly, samples were taken from surfaces within a few kT below the rotational barrier (e.g., $\varepsilon = -1, -2, -3$) in addition to the samples taken on the barrier surface ($\varepsilon = 0$). The reactive trajectories, i.e., $f \rightarrow b$, were divided into groups or "boxes," according to the magnitude of ε_i and ε_f, and the effective number of reactive trajectories in each box was then counted. The equilibrium transition rate is given by

$$R(\varepsilon_i, \varepsilon_f) = [f_k(\varepsilon)/(\Delta\varepsilon)^2] \cdot R_v(\varepsilon) \qquad (2.7)$$

where $(\Delta\varepsilon)^2$ is the size of the box, ε is the position of the surface from which samples were taken, the subscript k specifies the box defined by ε_i, ε_f and $(\Delta\varepsilon)^2$, and

$$f_k(\varepsilon) = \sum_{j=1}^{N_o} (x_{jk}/n_j)/N_o(\varepsilon) \qquad (2.8)$$

is the effective number of reactive trajectories falling in the k-th box. Here, $x_{jk} = 1$ if the trajectory is reactive, $x_{jk} = 0$ if it is nonreactive, and n_j is the number of crossings of that trajectory in the reactive direction (e.g., from free to bound, in the case of recombination).

As was observed previously, a separable form of the kernel $R(\varepsilon_i, \varepsilon_f)$ results in great simplification in solving the master equations. We found that the empirical form

$$R(\varepsilon_i, \varepsilon_f) = A G(\varepsilon_f) \exp(\alpha \varepsilon_f - \beta \varepsilon_i) \qquad (2.9)$$

was able to reproduce the relative numerical distribution of $R(\epsilon_i, \epsilon_f)$ with sufficient accuracy. In Equation (2.9) A, α, and β are constants and $G(\epsilon_f)$ is a relatively slowly varying function.

It was observed from the map of the relative numerical distirbution of $R(\epsilon_i, \epsilon_f)$ that the kernel exhibits a sharp maximum along the diagonal $\epsilon_i = \epsilon_f$, dies off very rapidly away from the diagonal, and varies relatively slowly along the diagonal. Thus the fitting was made easier by rotating the energy coordinates and expressing the kernel in the form $R(\Delta, \bar{\epsilon})$, where

$$\Delta = |\epsilon_i - \epsilon_f| \tag{2.10a}$$

is the absolute value of the energy transfer and

$$\bar{\epsilon} = (\epsilon_i + \epsilon_f)/2 \tag{2.10b}$$

is the mean of the initial and final energies. The symmetry of $R(\epsilon_i, \epsilon_f)$ in ϵ_i and ϵ_f requires that

$$R(\epsilon_i, \epsilon_f) = R(\Delta, \bar{\epsilon}) . \tag{2.11}$$

Thus, in view of the kernel's rapid decay with Δ and the fact that the function $G(\epsilon_f)$ is relatively slowly varying, we can write

$$R(\Delta, \bar{\epsilon}) = A\, G(\bar{\epsilon})\, \exp(-a\Delta - b\bar{\epsilon}) \tag{2.12}$$

with

$$\alpha = a - b/2, \text{ and } \beta = a + b/2 . \tag{2.13}$$

Various moments of the energy transfer with respect to the kernel were used in the fitting procedure (see also Section IIIB). The m-th moment of energy transfer $(\epsilon_i - \epsilon_f)$ with respect to $R(\epsilon_i, \epsilon_f), R_v(\epsilon)$ is defined as

$$K_m(\varepsilon) = \int_{-\infty}^{\varepsilon} d\varepsilon_f \int_{\varepsilon}^{\infty} d\varepsilon_i [R(\varepsilon_i, \varepsilon_f)/\mathcal{R}_v(\varepsilon)] (\varepsilon_i - \varepsilon_f)^{m-1} . \qquad (2.14)$$

By substituting Equations (2.7) and (2.8) into Equation (2.14) and evaluating the integral by Monte Carlo methods, we obtain

$$K_m(\varepsilon) = \sum_{j=1}^{N_o} (x_j/n_j) (\varepsilon_i - \varepsilon_f)_j^{m-1}/N_o(\varepsilon) \qquad (2.15)$$

where $x_j = 1$ if the trajectory is reactive, and $x_j = 0$ otherwise. This is the equation used in the actual calculation of the moments $K_m(\varepsilon)$ from data generated by trajectory calculations.

Now, the equilibrium one-way crossing rate $\mathcal{R}(\varepsilon)$ is defined as

$$\mathcal{R}(\varepsilon) \equiv \int_{-\infty}^{\varepsilon} d\varepsilon_f \int_{\varepsilon}^{\infty} d\varepsilon_i R(\varepsilon_i, \varepsilon_f) . \qquad (2.16)$$

Rotating the energy coordinates to $[\Delta, \bar{\varepsilon}]$ and using Equation (2.12), we obtain

$$\mathcal{R}(\varepsilon) \approx A G(\varepsilon) \exp(-b\varepsilon)/(a^2 - b^2/4) \qquad (2.17)$$

where $G(\bar{\varepsilon})$ has been expanded about ε and small terms dropped.

In addition, we found by plotting (N/N_o) versus ε, that the form

$$N(\varepsilon)/N_o(\varepsilon) = C \exp(p\varepsilon) \qquad (2.18)$$

with both C and p constant, correlates the numerical data reasonably well. By combining Equations (2.5), (2.17), and (2.18), we obtain

$$\mathcal{R}_v(\varepsilon) \exp(\varepsilon)/\mathcal{R}_v(0) = G(\varepsilon) \qquad (2.19)$$

$$b = 1 - p , \qquad (2.20)$$

and $\qquad A/\mathcal{R}_v(0) = C(a^2 - b^2/4) . \qquad (2.21)$

The moments defined by Equation (2.14) can then be evaluated by using the above relationships as follows:

$$K_m(\varepsilon) = A[G(\varepsilon) \exp(-\varepsilon)R_v(0)]^{-1} \int_{\varepsilon-\Delta/2}^{\varepsilon+\Delta/2} d\bar{\varepsilon} \int_0^\infty d\Delta \ G(\bar{\varepsilon}) \exp(-a\Delta-b\bar{\varepsilon}) \ \Delta^{m-1}. \quad (2.22)$$

When $a \gg b/2$, a good approximation is

$$K_m(\varepsilon) \approx C \ m! \ a^{1-m} \exp[(1-b)\varepsilon] \qquad (2.23)$$

The ratios of these moments are independent of the energy ε, and the parameter a may be obtained directly from any of these ratios. However, since we anticipate from the diffusion analysis[7] that it is the first and the second moments which are most important for determining the steady-state rate coefficients, we have used the value of a given by the ratio $2K_1/K_2$.

Having obtained a separable form for the transition kernel, we can now proceed to solve the steady-state master equations which will yield the nonequilibrium correction factor. Keck and Carrier[7] showed that the steady-state master equation can be transformed exactly into an equivalent diffusion equation and then solved subject to the appropriate boundary conditions. For the case of the separable kernel, they assumed

$$R(\varepsilon_i, \ \varepsilon_f) = \begin{cases} r_2(\varepsilon_i) \ r_1(\varepsilon_f) \ ; \ \varepsilon_i > \varepsilon_f \\ r_2(\varepsilon_f) \ r_1(\varepsilon_i) \ ; \ \varepsilon_f > \varepsilon_i \end{cases} \qquad (2.24)$$

and

$$R(c, \ \varepsilon) = r_1(\varepsilon) \ r_c \qquad (2.25)$$

where r_c is a constant and

$$R(c, \ \varepsilon) = \int_0^\infty R(\varepsilon', \ \varepsilon) \ d\varepsilon' \qquad (2.26)$$

is the equilibrium recombination (or dissociation) rate.

By solving the equivalent diffusion equation, they obtained the expression for the nonequilibrium correction factor

$$k/k_e = \{\mathcal{R}(0) \ [\int_{-\delta}^{0} WZ^{-2} \ d\epsilon + r_2(0)/(r_c Z(0))]\}^{-1} \qquad (2.27)$$

where $\mathcal{R}(0)$ is the one-way equilibrium flux of molecules across the energy surface $\epsilon = 0$, defined in Equation (2.16),

$$W(\epsilon) = r_2(dr_1/d\epsilon) - r_1(dr_2/d\epsilon) \qquad (2.28)$$

is the Wronskian of r_2 and r_1 ,

$$Z(\epsilon) = r_2(\epsilon) \int_{-\delta}^{\epsilon} r_1(\epsilon') \ d\epsilon' + r_1(\epsilon)[\int_{\epsilon}^{0} r_2(\epsilon') \ d\epsilon' + r_c] \qquad (2.29)$$

is the equilibrium collision rate, and $\delta = D/kT$ is the dimensionless potential-well depth of the molecule.

Since we sampled trajectories for recombination, the condition, $\epsilon_i > \epsilon_f$, was satisfied in all cases. Thus, for the kernel given by Equation (2.9), we have

$$r_2(\epsilon_i) = \exp(-\beta\epsilon_i) \ , \ r_1(\epsilon_f) = A \ G(\epsilon_f) \ \exp(\alpha\epsilon_f) \qquad (2.30)$$

and

$$r_c = 1/\beta \ . \qquad (2.31)$$

By substituting Equations (2.34) and (2.35) into Equations (2.32) and (2.33) and then into Equation (2.31), we obtain

$$\frac{k}{k_e} \approx [1 - (\alpha/\beta)^2] \ [G(\epsilon^*)/G(0)] \qquad (2.32)$$

where ϵ^* is the location of the maximum of $G(\epsilon) \ \exp(-b\epsilon)$.

III. RESULTS

IIIA. The Interaction Potential

A Morse potential function is used to describe the two-body interaction between H and $C\ell$ as before,[4] with the same potential parameters; i.e., $D = 4.62$ eV(53600 °K), $r_e = 1.275$ Å, and $\beta = 1.87$ Å^{-1}. However, dumb-bell models as used before[3,6] for the three-body interaction potential are not well defined when V_{XM} and V_{YM} are considerably different and have attractive potential wells. To overcome this difficulty, we reverted to the use of the purely repulsive Mason-Vanderslice exponential interaction potential,[1,7,9]

$$V = A \exp(-r/\ell). \tag{3.1}$$

Then the dumb-bell model is defined as

$$V_3 = V_{XM} \quad \text{for } V_{XM} > V_{YM},$$
$$\text{and} \quad V_3 = V_{YM} \quad \text{for } V_{XM} < V_{YM}. \tag{3.2}$$

This change should not affect the results which are of concern here since we consider only dissociation rate measurements at high temperatures (2500 - 5000 °K), and it has been shown[3-5] that the potential well in V_3 has negligible effects on reaction rate coefficients at such elevated temperatures. Table I summarizes the parameters A_{iM} and ℓ_{iM} used in the present calculations.

IIIB. Reaction Rates

Table II shows the distribution of the three hundred trajectories sampled for the case of Ar + HCℓ at 2500 °K (kT/D = .0466) with $\epsilon = 0$, classified according to the nature of their end states (see Section IIA). The implications of Table II have already been discussed by Keck.[6] Of

course, as pointed out before, his empirical correlation formula for (N/N_o) does not apply to the present case. In addition, Keck's Table I for homonuclear molecules showed entries of comparable magnitude for $N(f|n|f)$ and $N(b|n|b)$; whereas, we found that $N(f|n|f) \gg N(b|n|b)$ for Ar + HCℓ. The reason for this difference will be explained in Section IV when we discuss details of the Ar + HCℓ trajectories.

The recrossing connection factor N/N_o for the various temperatures and surfaces sampled are plotted versus ε in Figure 1. No definite temperature dependence can be determined from the plot (Keck's previous results[2,6] also did not show any temperature effect on N/N_o). Although there is considerable scatter in the data, the least-squares fit line does give a reasonable representation of all the data points. The parameters $p = 0.26$, $b = 1 - p = 0.74$, and $C = [N(0)/N_o(0)] = 0.27$ are all obtained from this fitted line (see Equations (2.19) and (2.21)).

The various moments, $K_m(\varepsilon)$, as defined by Equation (2.14) were then calculated using Equation (2.15) and tabulated in Table III. The ratio $2K_1/K_2 \approx a$ (see Equations (2.26) and (2.27)) is also included in the table.

In order to complete the determination of the transition kernel, $R(\varepsilon_i, \varepsilon_f)$, and produce a map of its relative numerical distribution, we must first find the pre-exponential function $G(\varepsilon_f)$ (see Section IIB). Keck[2] found that the function

$$G(\varepsilon) = [1 - (-\varepsilon/\delta)^{1/2}]/[1 + (-\varepsilon/\delta)^{1/2}] \tag{3.3}$$

was able to represent his numerical calculations of $R_v(\varepsilon)/R_v(0)$ with sufficient accuracy, and we have used this form for $G(\varepsilon_f)$. The resulting

numerical distribution of $R(\varepsilon_i, \varepsilon_f)/R_v(0)$ is shown in Figure 2, again for Ar + HCl at 2500 °K. The figures in the boxes represent the mean value of $R(\varepsilon_i, \varepsilon_f)/R_v(0)$ for the box. Because of the sampling technique employed, each value of ε used in the calculations gives data in a quadrant that touches the diagonal $\varepsilon_i = \varepsilon_f$, at a value of $(\varepsilon_i + \varepsilon_f)/2 = \bar{\varepsilon} = \varepsilon$. Data in overlapping quadrants agreed within the statistical errors and were averaged to obtain the results shown. The total number of trajectories sampled was approximately three hundred for each value of $\varepsilon(\varepsilon = 0, -1, -2, -3)$. The results shown were calculated for $\varepsilon_i > \varepsilon_f$ (recombination); however, since $R(\varepsilon_i, \varepsilon_f)$ is symmetrical in ε_i and ε_f, the values for $\varepsilon_i < \varepsilon_f$, may be obtained by reflection in the diagonal $\varepsilon_i = \varepsilon_f$. As was pointed out in Section IIB, the map shows that $R(\varepsilon_i, \varepsilon_f)$ exhibits a sharp maximum ridge along $\varepsilon_i = \varepsilon_f$, which corresponds to zero energy transfer; this dies off rapidly as $|\varepsilon_i - \varepsilon_f|$ increases. Combining Equations (2.9) and (2.22), we obtain

$$R(\varepsilon_i, \varepsilon_f)/R_v(0) = C(a^2 - b^2/4) \, G(\varepsilon_f) \, \exp(\alpha\varepsilon_f - \beta\varepsilon_i) . \qquad (3.4)$$

Since all the parameters in Equation (3.2) have been obtained, we can use them to generate the function $R(\varepsilon_i, \varepsilon_f)/R_v(0)$. The parameter a used is the average of the four values of $2K_1/K_2$ in Table III. The result for $T = 2500$ °K is plotted in the upper left corner of Figure 2 as a contour map. We see that this map reproduces all the important features of the actual distribution, and the agreement in general is very good.

In Figure 3 we have plotted $[R(\Delta, \bar{\varepsilon})/R_v(0)]/[R(\bar{\varepsilon})/R(0)]$ versus Δ. The factor $[R(\bar{\varepsilon})/R(0)]$ is included for normalization purposes. The solid line passing through the bulk of the data points has a slope, $a = 1.79$,

as determined above (see Table III). It can be seen that for $\Delta < 0.5$, the data points deviate considerably from this line; however, the region around $\Delta \approx 1$, has the most important contribution in the determination of the nonequilibrium correction factor, and the line fits the data very well in this region.

We therefore conclude that our functional form for $R(\epsilon_i, \epsilon_f)$ and the associated parameters determined above lead to a very good representation of the transition kernel. At the same time, it is still simple enough so that the steady-state master equation can be solved analytically without the usual reliance on a great deal of numerical computation.

The nonequilibrium correction factors may now be calculated from Equations (2.13) and (2.36). The barrier rate coefficients are taken from Reference 4 and the results are summarized in Table IV for $T = 5000^\circ$, 3500°, and $2500\ ^\circ K$. It should be noted that for the results shown, the corresponding characteristic energy transfer in a collision is between $0.4\ kT$ and $0.6\ kT$. The statistical errors, based on one standard deviation, are estimated to be about 10 per cent for (N/N_o) and 20 per cent for (k/k_e).

Figure 4 is an Arrhenius plot of the measured (full lines and open points) and calculated (solid points) dissociation rate coefficients of $HC\ell$ in Ar. It shows that the present theoretical predictions are in excellent agreement both in terms of magnitude and temperature dependence with the experimental measurements of Seery and Bowman,[10] Fishburne,[11] and Jacobs, Cohen, and Giedt.[12] We should point out that the major temperature dependence of k_d is determined by the barrier rate coefficient k_d^B.

The correction factors (N/N_o) and (k/k_e) lower the rates and introduce an additional relatively weak temperature dependence to the rate coefficients. Error bars on the theoretical points show estimated statistical errors of $\pm$ 20 per cent.

IV. DISCUSSION

The Landau-Teller theory of vibrational relaxation,[13] as extended by Schwartz, Slawsky, and Herzfeld (SSH),[14] which considered vibrational-translational energy transfer, provided both a successful qualitative explanation and quantitative correlation of the vibrational relaxation rates of most of the homonuclear diatomic molecules which have been investigated. However, when applied to highly asymmetric heteronuclear diatomic molecules (e.g., HF and HCl), the theory predicted rates[15] several orders of magnitude slower than those observed experimentally.[16-20] This discrepancy led to the suspicion that rotational motion may be important in vibrational relaxation. Much work has been done in this respect, and it appears that by properly accounting for the rotational motion of the molecules, the very high vibrational relaxation rates for molecules such as HF and HCl, as well as the effects of deuteration, can now be explained and correlated. Detailed discussions and references on the topic of rotation-vibration coupling can be found in papers by Moore,[21] Chen and Moore,[22] and in a recent comment by Nikitin.[23]

According to the SSH theory, the efficiency of energy transfer for a collision depends on an "adiabaticity factor," $f(\omega\tau)$, where ω is the vibrational frequency of the molecule and τ is the "effective time" of the collision, i.e., the time available for energy transfer. In the theory, the relative velocity between the center of mass of the molecule

and the collision partner is used to estimate τ; thus $\tau \alpha (\mu_{XY,M})^{1/2}$, where $\mu_{XY,M} = m_{XY} m_M / (m_{XY} + m_M)$ is the effective reduced mass of the collision complex. Such reasoning as this led Keck to seek a correlation of the recrossing correction factors (N/N_o) for homonuclear molecules and various collision partners on the basis of the adiabaticity parameter, $\omega \tau \alpha (\mu_{XY,M}/\mu_{XY})^{1/2}$. However, for such systems as HCℓ + Ar, the hydrogen atom moves much more rapidly than does either the Cℓ or Ar atoms due to its much lighter mass. As can be seen in the trajectories shown in Figure 5, the essential motion of the H atom is that of rotation about the Cℓ atom. Thus a more correct collision time for these heteronuclear systems is determined by the motion of the H atom relative to the Ar atom and not by the relative motion of the HCℓ and Ar. Consequently, the quantity $\mu_{HC\ell,Ar}$ in the SSH theory should more properly be replaced by $\mu_{HAr} = m_H m_{Ar}/(m_H + m_{Ar}) \approx m_H$, the reduced mass of the H-Ar collision. This point is clearly illustrated by the three reactive trajectories we plotted in Figure 5. The duration of the strong interaction, where most of the energy and momentum transfers occur, is indicated by the thicker lines on the trajectories. We see that during this period of strong interaction (corresponding to the effective collision time), the Ar atom hardly moves relative to the Cℓ atom whereas, by rotation, the H atom passes completely through the reaction zone. Since the adiabaticity factor $f(\omega\tau)$ has a dependence given by the factor $\exp(-\alpha \omega \tau)^{\beta}$, where both α and β are of order unity, the change from $\mu_{XY,M}$ to μ_{XM} increases the magnitude of the adiabaticity parameter to order unity for such systems as HCℓ + Ar and thus raises the calculated vibrational relaxation

rates by several orders of magnitude in agreement with experimental
observations. Additional trajectory calculations for the heternuclear
molecules using different collision partners are required before we are
in a position to deduce correlation formulas for the correction factors
similar to those obtained by Keck.

The inner dashed circles in Figure 5 indicate the equilibrium
separation for $HC\ell$ molecules, the outer dashed circles are the posi-
tions, z_2, of the rotational maximum evaluated at the end of the colli-
sion. In general the following observations can be made about the $HC\ell$-Ar
collisions:

1. For non-reactive collisions (unlike those shown in Figure 5) the Ar
   atom acts as a block which prevents the H atom from reaching the $C\ell$
   atom by virtue of its position between the $C\ell$ and H atoms; i.e.,
   $r_{HC\ell} > r_{HAr}$. These collisions are, in fact, automatically excluded
   from our samples since they never reach the reaction zone.

2. On the other hand, participation of Ar in the collision is necessary
   to take away the excess energy from $H \cdot C\ell$ and thereby effect a recombina-
   tion. Thus typical reactive trajectories, such as those shown in
   Figure 5, may be divided into three different phases:

   (i) The H atom approaches the $C\ell$ atom from the opposite side to
       the Ar atom with little or no interference from Ar.

   (ii) Due to the action of the strong attractive valence forces
        between H and $C\ell$, the H atom cuts into a line joining Ar and
        $C\ell$ and transfers energy and momentum to Ar. This is the zone
        of strong interaction (thicker line on the trajectories) during

which most of the energy and momentum exchanges are effected.
We note that at the beginning of this reaction zone, the Ar
atom is usually very near the turning point with respect to
the $C\ell$ atom so that its kinetic energy is very low.

(iii) The H atom, having lost sufficient energy, becomes bound to
$C\ell$ atom and then proceeds to vibrate and rotate about the
latter; whereas, the Ar atom moves away from $HC\ell$ molecule
with an increased velocity.

We should point out that for convenience of representation in two
dimensions, the trajectories shown in Figure 5 have all three particles
moving in the same plane. However, our calculations were, in general,
three dimensional.

In Section IIIB we noted that $N(f|n|f) \gg N(b|n|b)$ for Ar + $HC\ell$
collisions; whereas, Keck[6] obtained $N(f|n|f) \approx N(b|n|b)$ for all the
homonuclear molecules he investigated. The reason for this difference
can now be explained. The variational reaction rate calculations show
that the contribution to the reaction rate from collisions with the $C\ell$
end of the molecule is negligible. In addition, both Ar and $C\ell$ can be
regarded as almost stationary while the hydrogen atom moves about at
high average velocities. Therefore, most of the energy exchanges that
may change the state of $HC\ell$ must come from the H-Ar collision, with very
little direct influence from the $C\ell$ atom. Our sampling procedure ensures
that the molecule must be on the energy surface $H - B = 0$ at a certain
time $t = t_o$, and the trajectory must cross that surface at t_o with a
negative slope (for recombination); i.e., the molecule must be in a free

state $(H - B > 0)$ at some time $t < t_o$ and must be losing energy to the Ar
atom. Consider the case in which the H atom was initially bound to the
Cℓ atom at $t << t_o$. The result of the H + Ar collision would be either
(a) a net loss of energy from H to Ar, with the HCℓ molecule remaining
bound, or (b) a net gain of energy by H from Ar, making H free from Cℓ.
Obviously trajectories (a) are not sampled by our procedure since they
do not cross the surface $H - B = 0$; nor do trajectories (b) cross the
surface in the desired direction since, once the H atom becomes free
after a collision with the Ar atom, its rapid motion will carry it away
from the Cℓ + Ar system. Thus no further significant energy transfer
between H and Ar, which would change the state of HCℓ, is probable;
i.e., HCℓ remains free, and those trajectories are not sampled. On the
other hand, it is easy to see that if H was initially free at $t << t_o$,
its collision with Ar would produce f → b trajectories that satisfy our
sampling requirements. Consequently, the result $N(f|n|f) >> N(b|n|b)$
for Ar + HCℓ collisions is expected.

For homonuclear molecules, the outcome of case (b), above, may be
quite different. The b → f transition would be a result of the collision
between one end of the molecule and the third body, as before. However,
rotation of the molecule may bring the other end into a collision with
the third body and could thereby produce a f → b transition. These
trajectories (b → f → b) satisfy our sampling requirements, and $N(f|n|f)$
and $N(b|n|b)$ may therefore have comparable magnitudes. Typical trajectories
of this kind which illustrates our point will be presented when we report
our work on homonuclear molecules.

It should be noted that the features of the collision mechanics discussed above would be suppressed if only colinear collisions were considered. Thus the one-dimensional approximation sometimes used in theoretical analyses of this nature presents a picture which is very different from what actually is the case for both homonuclear and heternuclear molecules.

For a collision to be reactive (consider recombination), the molecule must start in a free state and end in a bound state. The corresponding energy changes must be such that $H - B < 0$, where H is the Hamiltonian of the molecule, and B is the height of the rotational barrier. Figure 6 shows a distribution plot of ΔH and ΔB for 101 reactive trajectories out of the three hundred trajectories sampled for $HC\ell$ + Ar at 2500 ^{o}K on the surface $S(0)$. It is apparent that recombination (the change from $H - B > 0$ to $H - B < 0$) is achieved by two equally important mechanisms, i.e., reducing H and/or increasing B. Our work on homonuclear molecules (to be reported separately), on the other hand, shows that most recombinations are achieved by reducing H. This furnishes further evidence that rotational energy transfer in asymmetric molecules plays a relatively important part in chemical reactions. The energy transfers ΔH and ΔB for the three trajectories shown in Figure 5 are indicated by the filled points in Figure 6. They represent different ratios of $\Delta B/\Delta H$.

The calculations presented in this paper are for one system (Ar + $HC\ell$) and over a limited (high) temperature range (2500° - 5000 ^{o}K). Work on other diatomic molecules is in progress which will cover the high temperature dissociation region and the low temperature recombination region. A

number of interesting questions can be answered by such calculations;
e.g., what is the physical interpretation of the parameters α and β
involved in the equilibrium transition rates, and what will be the con-
tribution from the "complex" mechanism to the overall recombination
rate coefficient at low temperatures? In any event, the agreement between
the theoretically predicted dissociation rate coefficients and experimental
measurements for the case of HCℓ + Ar presented here undoubtedly provides
another successful test for the classical modified phase-space theory
of reaction rates.

REFERENCES

1. J. C. Keck, J. Chem. Phys. 32, 1035 (1960).

2. J. C. Keck, Advances Chem. Phys. 13, 85 (1967).

3. V. H. Shui, J. P. Appleton, and J. C. Keck, J. Chem. Phys. 33 2547 (1970).

4. V. H. Shui, J. P. Appleton, and J. C. Keck, Symp. Combust. 13th, Salt Lake City, Utah, 19 (1971).

5. V. H. Shui and J. P. Appleton, J. Chem. Phys. 55, 3126 (1971).

6. J. C. Keck, Discussions Faraday Soc. 33, 173 (1962).

7. J. C. Keck and G. F. Carrier, J. Chem. Phys. 43, 2284 (1965).

8. P. Mansbach and J. C. Keck, Phys. Rev. 181, 275 (1969).

9. E. A. Mason and J. T. Vanderslice, J. Chem. Phys. 28, 432 (1958).

10. D. J. Seery and C. T. Bowman, J. Chem. Phys. 48, 4314 (1968).

11. E. S. Fishburne, J. Chem. Phys. 45, 4053 (1966).

12a. T. A. Jacobs, N. Cohen, and R. R. Giedt, J. Chem. Phys. 46, 1958 (1967).

12b. R. R. Giedt and T. A. Jacobs, J. Chem. Phys. 55, 4144 (1971).

13. L. Landau and E. Teller, Phys. Zeit. Sowjetunion 10, 34 (1936).

14a. R. N. Schwartz, Z. I. Slawsky, and K. F. Herzfeld, J. Chem. Phys. 20, 1591 (1952).

14b. R. N. Schwartz and K. R. Herzfeld, ibid. 22, 767 (1954).

15. K. F. Herzfeld and T. A. Litovitz, Absorption and Dispersion of Ultrasonic Waves (Academic, New York, 1959).

16. C. C. Chow and E. F. Green, J. Chem. Phys. 43, 324 (1965).

17. W. D. Breshears and P. F. Bird, J. Chem. Phys. 50, 333 (1969).

18. W. D. Breshears and P. F. Bird, J. Chem. Phys. 51, 3660 (1969).

19. W. D. Breshears and P. F. Bird, J. Chem. Phys. 52, 999 (1970).

20. J. R. Airey and S. F. Fried, Chem. Phys. Letters, 8, 23 (1971).

21. C. B. Moore, J. Chem. Phys. 43, 2979 (1965).

22. H. L. Chen and C. B. Moore, J. Chem. Phys. 54, 4072 (1971).

23. E. E. Nikitin, Comments on Atomic and Molecular Phys. 2, 59 (1970).

TABLE I. Mason-Vanderslice Potential Parameters

System	A(eV)	$\ell(\overset{o}{A})$
Ar + H	268	0.35
Ar + Cℓ	1060	0.35

TABLE II. Distribution of trajectories with respect to class of reaction and number of traversals of the barrier surface ($\varepsilon = 0$), for Ar + HCl at 2500 $^\circ$K(kT/D = 0.047)

Class n	N 1	2	3	Total
(f|n|b)	91	8		99
(f|n|f)	142	9	2	153
(b|n|b)	10	4		14
(b|n|f)	16	2		18
Total				284

Recrossing correction factor

$(N/N_o) = (91 + 8/2)/284 = 0.33$

TABLE III. Moments $[K_m(\varepsilon)]$ for Ar + HCl

$T(^{o}K)$	kT/D	ε	K_0	K_1	K_2	$2K_1/K_2$
5000	.093	0	1.09	.245	.159	3.08
		-1	.501	.182	.158	2.30
		-2	.505	.102	.079	2.58
		-3	.348	.080	.043	3.72
		mean				2.92
3500	.065	0	1.34	.233	.174	2.68
		-1	.693	.190	.242	1.57
		-2	.321	.130	.130	2.00
		-3	.464	.112	.095	2.36
		mean				2.15
2500	.047	0	1.71	.331	.332	1.99
		-1	.675	.192	.247	1.56
		-2	.555	.202	.241	1.68
		-3	.364	.157	.162	1.94
		mean				1.79

TABLE IV. Dissociation Rate Coefficients for Ar + HCl

$T(^oK)$	$\frac{kT}{D}$	k_d^B	$\frac{N}{N_o}$	b	a	$\frac{k}{k_e}$	k_d
5000	.093	5.69^{-13}	.27	.74	2.92	.30	4.55^{-14}
3500	.065	7.26^{-15}	.27	.74	2.15	.42	8.27^{-16}
2500	.047	1.81^{-17}	.27	.74	1.79	.50	2.44^{-18}

k_d^B and k_d have units cm^3 $molecule^{-1}$ sec^{-1}.

FIGURE CAPTIONS

Figure 1 Recrossing correction factors, N/N_0 versus energy of the
surface from which samples were taken. $\bullet$, T = 5000 ^{O}K;
$\ominus$, T = 3500 ^{O}K; $\bigcirc$, T = 2500 ^{O}K. Solid line is the best
least-squares fit for all points. The slope of this line
determines the parameter b.

Figure 2 Map of numerical distribution of the function $R(\varepsilon_i, \varepsilon_f)/\mathcal{R}_v(0)$,
where $R(\varepsilon_i, \varepsilon_f)$ is the equilibrium transition rate and $\mathcal{R}_v(0)$
is the variational rate for the surface $\varepsilon = 0$. The contour
map, calculated from Equation (3.2) using the fitted parameters,
is plotted in the upper left corner to avoid overcrowding the
figure. Comparison may be done by reflection through the
diagonal $\varepsilon_i = \varepsilon_f$.

Figure 3 The function $[R(\Delta, \bar{\varepsilon})/\mathcal{R}_v(0)]/[\mathcal{R}(\bar{\varepsilon})/\mathcal{R}(0)]$ is plotted versus Δ,
the absolute value of energy transfer. $\bullet$, $\bar{\varepsilon} = 0$; $\bigcirc$, $\bar{\varepsilon} = -1$;
$\blacktriangle$, $\bar{\varepsilon} = -2$; $\triangledown$, $\bar{\varepsilon} = -3$. The factor $[\mathcal{R}(\bar{\varepsilon})/\mathcal{R}(0)]$ is included
for normalization purposes so that the data can be better
represented by a single line. The solid line which passes
through the bulk of the data has a slope a taken from Table III.
See text, Section IIIB.

Figure 4 Comparison between theoretical predictions of the dissociation
rate coefficient and experimental measurements, as a function
of T. $\blacklozenge$, theoretical predictions; $\bigcirc$, Seery et al; (F),
Fishburne; (J), Jacobs et al; dashed curve represents the
theoretical barrier rate coefficients.

Figure 5 Typical reactive trajectories. The thicker lines on the
trajectories indicate zones of strong interaction.
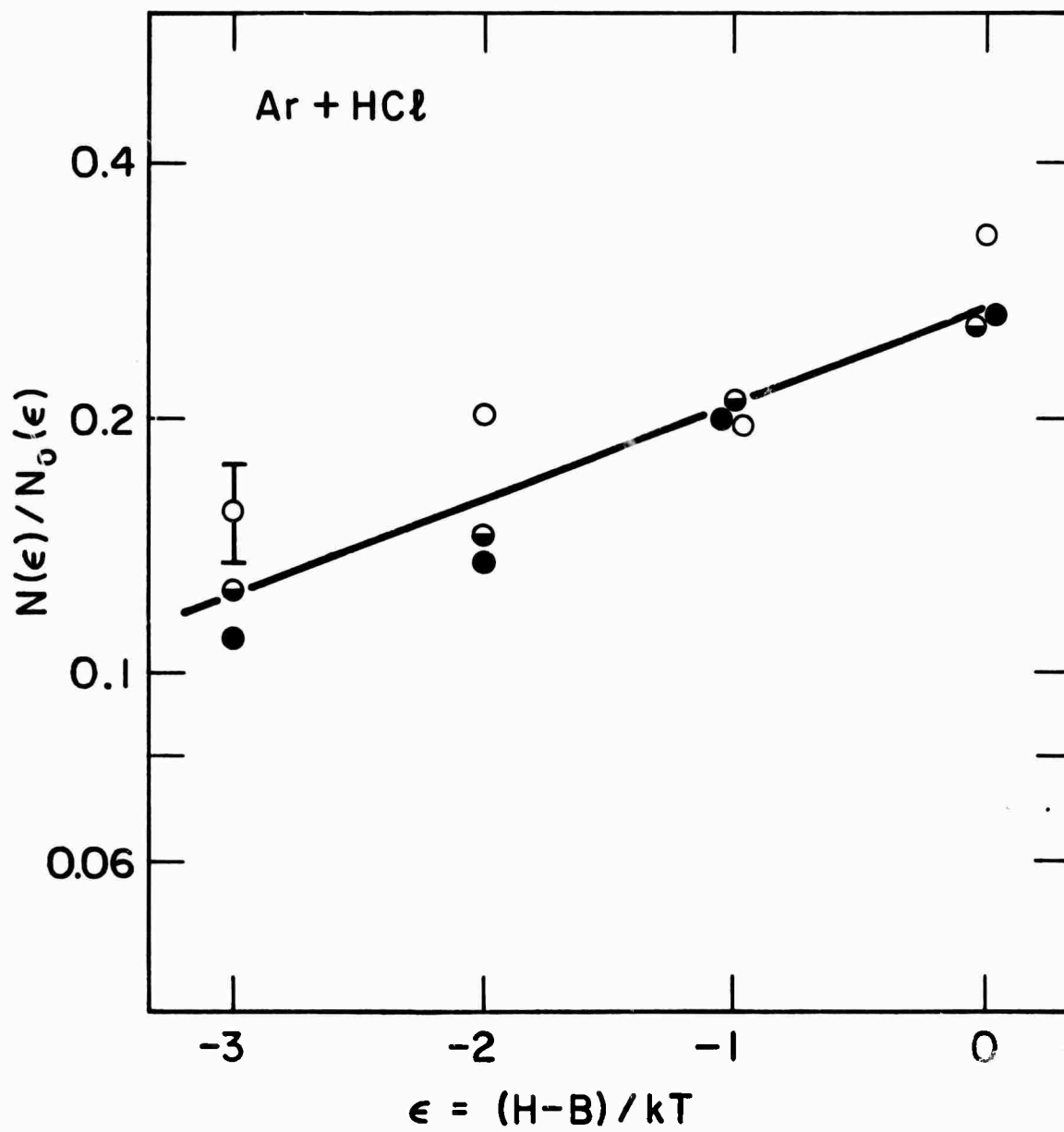
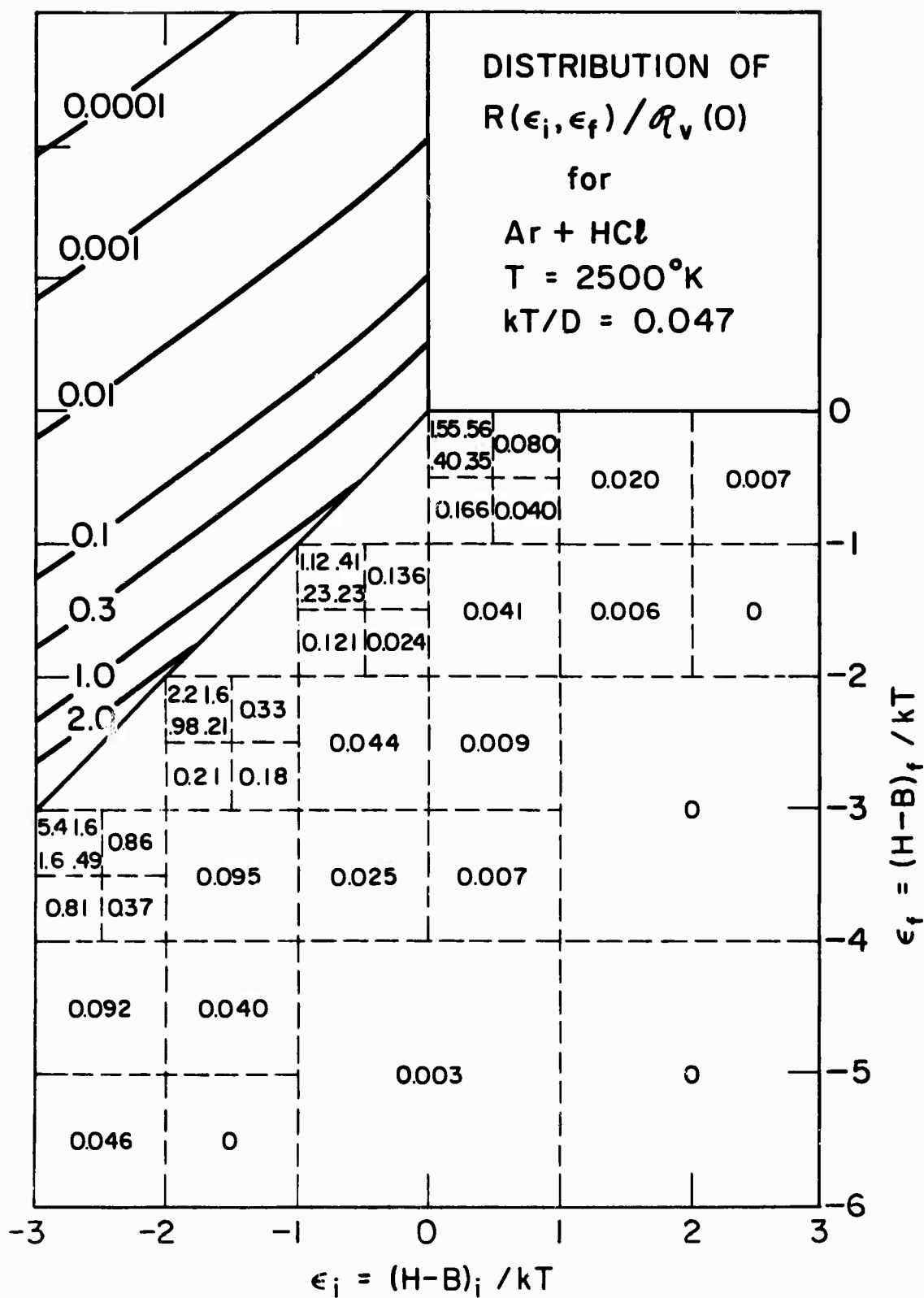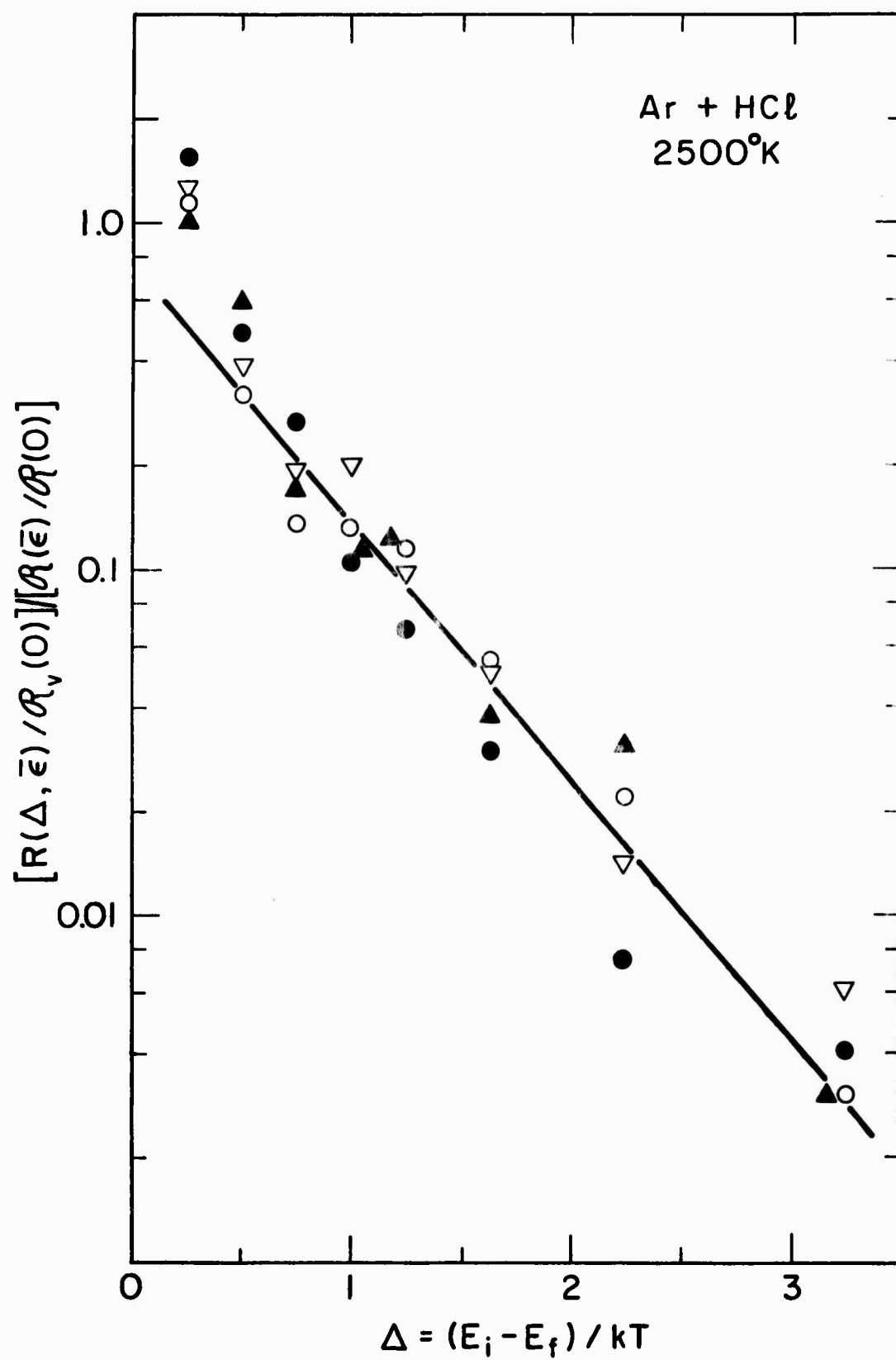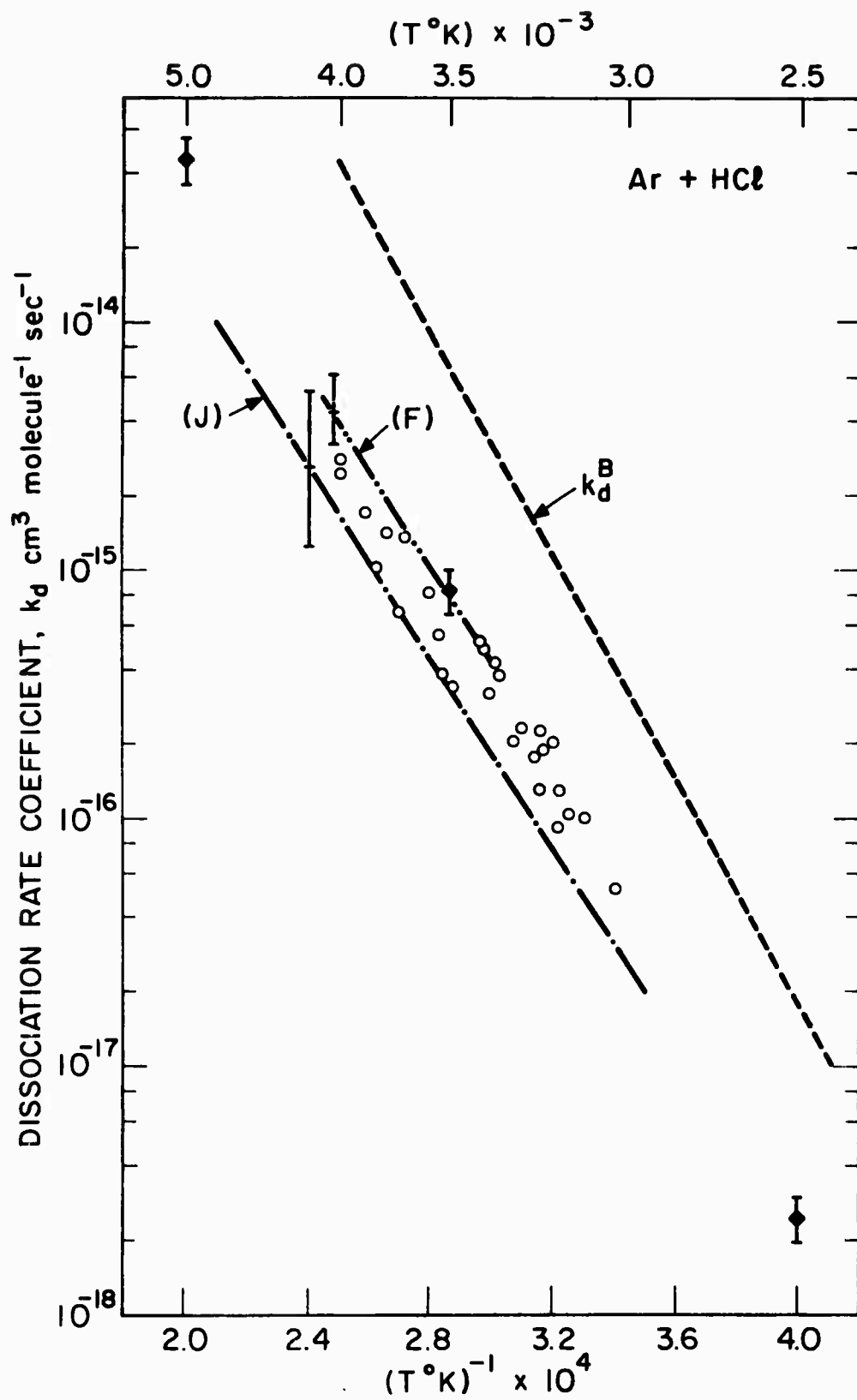Figure 6 Distribution plot of reactive trajectories in the [ΔH, ΔB]
plane.

FIGURE 1

FIGURE 2

FIGURE 3

FIGURE 4

FIGURE 5

FIGURE 6